



Electron dynamics in a subproton-gyroscale magnetic hole

Daniel J. Gershman, John C. Dorelli, Adolfo F. Viñas, Levon A. Avanov, Ulrik Gliese, Alexander C. Barrie, Victoria Coffey, Michael Chandler, Charles Dickson, Elizabeth A. Macdonald, et al.

► To cite this version:

Daniel J. Gershman, John C. Dorelli, Adolfo F. Viñas, Levon A. Avanov, Ulrik Gliese, et al.. Electron dynamics in a subproton-gyroscale magnetic hole. *Geophysical Research Letters*, 2016, 43, pp.4112-4118. 10.1002/2016GL068545 . insu-03670244

HAL Id: insu-03670244

<https://insu.hal.science/insu-03670244>

Submitted on 17 May 2022

HAL is a multi-disciplinary open access archive for the deposit and dissemination of scientific research documents, whether they are published or not. The documents may come from teaching and research institutions in France or abroad, or from public or private research centers.

Copyright

L'archive ouverte pluridisciplinaire **HAL**, est destinée au dépôt et à la diffusion de documents scientifiques de niveau recherche, publiés ou non, émanant des établissements d'enseignement et de recherche français ou étrangers, des laboratoires publics ou privés.

RESEARCH LETTER

10.1002/2016GL068545

Special Section:

First results from NASA's
Magnetospheric Multiscale
(MMS) Mission

Key Points:

- MMS data can resolve kinetic-scale structure in space plasmas
- Agyrotropic electrons carry current in a subproton-scale magnetic hole
- Current-carrying electrons have gyroradii above the thermal gyro radius

Correspondence to:

D. J. Gershman,
daniel.j.gershman@nasa.gov

Citation:

Gershman, D. J., et al. (2016), Electron dynamics in a subproton-gyroscale magnetic hole, *Geophys. Res. Lett.*, 43, 4112–4118, doi:10.1002/2016GL068545.

Received 4 MAR 2016

Accepted 8 APR 2016

Accepted article online 11 APR 2016

Published online 7 MAY 2016

Electron dynamics in a subproton-gyroscale magnetic hole

Daniel J. Gershman^{1,2}, John C. Dorelli², Adolfo F. Viñas², Levon A. Avanov^{1,2}, Ulrik Giiese^{2,3}, Alexander C. Barrie^{2,4}, Victoria Coffey⁵, Michael Chandler⁵, Charles Dickson², Elizabeth A. MacDonald², Chad Salo², Matthew Holland², Yoshifumi Saito⁶, Jean-Andre Sauvaud^{7,8}, Benoit Lavraud^{7,8}, William R. Paterson², Roy Torbert^{9,10}, Li-Jen Chen², Katherine Goodrich¹¹, Christopher T. Russell¹², Robert J. Strangeway¹², Barbara L. Giles², Craig J. Pollock², Thomas E. Moore², and James L. Burch¹³

¹Department of Astronomy, University of Maryland, College Park, Maryland, USA, ²NASA Goddard Space Flight Center, Greenbelt, Maryland, USA, ³SGT Inc., Greenbelt, Maryland, USA, ⁴Millenium Engineering and Integration Company, Arlington, Virginia, USA, ⁵NASA Marshall Space Flight Center, Huntsville, Alabama, USA, ⁶JAXA Institute of Space and Astronautical Science, Sagamihara, Japan, ⁷Institut de Recherche en Astrophysique et Planétologie, Université de Toulouse, Toulouse, France, ⁸Centre National de la Recherche Scientifique, UMR 5277, Toulouse, France, ⁹Physics Department, University of New Hampshire, Durham, New Hampshire, USA, ¹⁰Southwest Research Institute, Durham, New Hampshire, USA, ¹¹Astrophysical and Planetary Sciences, University of Colorado Boulder, Boulder, Colorado, USA, ¹²Department of Earth, Planetary, and Space Sciences, University of California, Los Angeles, California, USA, ¹³Southwest Research Institute, San Antonio, Texas, USA

Abstract Magnetic holes are ubiquitous in space plasmas, occurring in the solar wind, downstream of planetary bow shocks, and inside the magnetosphere. Recently, kinetic-scale magnetic holes have been observed near Earth's central plasma sheet. The Fast Plasma Investigation on NASA's Magnetospheric Multiscale (MMS) mission enables measurement of both ions and electrons with 2 orders of magnitude increased temporal resolution over previous magnetospheric instruments. Here we present data from MMS taken in Earth's nightside plasma sheet and use high-resolution particle and magnetometer data to characterize the structure of a subproton-scale magnetic hole. Electrons with gyroradii above the thermal gyroradius but below the current layer thickness carry a current sufficient to account for a ~10–20% depression in magnetic field magnitude. These observations suggest that the size and magnetic depth of kinetic-scale magnetic holes is strongly dependent on the background plasma conditions.

1. Introduction

Linear magnetic holes are discrete and localized diamagnetic depressions in the magnetic field. Increased perpendicular ion pressures observed inside of these structures indicate that particle heating occurs as part of their formation and evolution. These ubiquitous structures were first identified in the solar wind by *Turner et al.* [1977] and have been shown to exist on scales that range from $\sim 10^1$ to 10^3 proton gyroradii [*Tsurutani et al.*, 1992; *Winterhalter et al.*, 1994; *Stevens and Kasper*, 2007]. Similar magnetic holes have been reported in planetary magnetosheaths, cometary plasmas, and at border of the heliosphere [*Hasegawa*, 1969; *Russell et al.*, 1987; *Cattaneo et al.*, 1998; *Tsurutani et al.*, 2011]. The investigation of these magnetic holes and their formation processes leads to insights into local plasma dynamics and energization at different scales.

Multispacecraft observations revealed these magnetic holes to be quasi one-dimensional structures, where the edges of the magnetic holes are planar currents that extend many times their apparent thicknesses [*Fitzenreiter and Burlaga*, 1978]. The most commonly invoked formation mechanism of linear magnetic holes is the mirror-mode instability, where in thermally dominated (i.e., high β) plasmas, strong temperature anisotropy can give rise to "hole-like" signatures in the density [*Winterhalter et al.*, 1994]. Because the temperature anisotropy observed inside these structures is nearly always mirror stable, it is often suggested that the structures have formed elsewhere and evolved to their as-measured form [*Stevens and Kasper*, 2007; *Russell et al.*, 2008; *Amariutei et al.*, 2011]. An alternative proposed formation mechanism is from solitary waves, where steepened magnetohydrodynamic waves generate large-scale depletions in the magnetic field [*Buti et al.*, 2001; *Tsurutani et al.*, 2002].

Recent studies near Earth's neutral sheet leveraging multispacecraft observations have revealed magnetic holes with subproton-gyroradius sizes [*Ge et al.*, 2011; *Sun et al.*, 2012; *Sundberg et al.*, 2015]. These structures are characteristically different than their planar solar wind and magnetosheath counterparts, exhibiting

two-dimensional cylindrical geometry [Sundberg et al., 2015]. Here it is the increased perpendicular electron pressure that is observed inside the structures, reducing the ambient magnetic field strength by ~10–20% [Sun et al., 2012]. These holes have been observed in both quiet and active times near the central current sheet [Sundberg et al., 2015] and have been associated with the dissipation of energy from dipolarization fronts in the magnetotail [Ge et al., 2011; Balikhin et al., 2012].

Recent particle-in-cell (PIC) simulations [Haynes et al., 2015; Roytershteyn et al., 2015] of turbulent relaxation have demonstrated the near-spontaneous formation of so-called “electron vortex-magnetic holes”, where a small population of trapped electrons generates an azimuthal current that surrounds these structures. Large amplitude fluctuations of the magnetic field such as those generated by magnetic reconnection in the magnetotail may seed this formation process. Roytershteyn et al. [2015] found that ~90° pitch angle electrons between 1 and 3 times the thermal velocity should carry the azimuthal current in kinetic-scale magnetic holes. Observations from Cluster [Sun et al., 2012; Sundberg et al., 2015] suggest an enhancement of perpendicular electron fluxes inside magnetic holes consistent with these predictions, but low time resolution limited the characterization of the current layer.

The Fast Plasma Investigation (FPI) suite on the Magnetospheric Multiscale (MMS) mission provides high time resolution observations of the full three-dimensional velocity distribution functions of electrons (30 ms) and ions (150 ms) in Earth's magnetosphere [Pollock et al., 2016]. Although its first main science phase targets the dayside magnetopause, during commissioning MMS spent several orbits transiting the central plasma sheet in the magnetotail. On 7 May 2015, MMS3 passed through the center of a subproton-scale magnetic hole yielding unprecedented particle observations of its structure. We will use high-resolution plasma data to characterize the electron current layer of a kinetic-scale magnetic hole for the first time in section 2. In section 3, we will further analyze particle velocity distribution function data to identify the specific population of electrons that generate and sustain the reduction in the magnetic field magnitude. Finally, these observations will be placed in context with previous data analysis and modeling studies in section 4.

2. MMS Observations of a Subproton-Scale Magnetic Hole

MMS was launched in March 2015 and was commissioned in the nightside magnetosphere. Fluxgate magnetometer (FGM) data on all four observatories were available shortly after launch [Russell et al., 2016] whereas FPI conducted its first science operations on 7 May 2015 on MMS3. During this orbit, the MMS constellation passed through the central plasma sheet near-local midnight and a downtail distance of ~12 Earth radii, where MMS3 passed nearly through the center of a subproton-scale magnetic hole (Figure 1). The spacecraft were in a string-of-pearls configuration with nominal separation of ~160 km. Although limited to plasma observations from only a single spacecraft, we leverage high-resolution data from MMS3 to characterize the current layer of a subproton-scale magnetic hole for the first time. MMS/FPI will not regularly sample the plasma sheet at this local time until Phase 2 of the mission, which starts in early 2017. In their highest time resolution mode, FPI's Dual Electron Spectrometer (DES) and Dual Ion Spectrometer (DIS) sensors provide full three-dimensional electron and ion velocity distribution functions between 10 eV and 30 keV every 30 ms and 150 ms, respectively. Because this event was observed early in commissioning, there is additional uncertainty in the vector magnetic field of approximately ~0.05 nT in the spin-plane components (X , Y) and ~0.5 nT in the axial field component (Z). These uncertainties result in an angular difference of ~1–2° and a change in magnetic pressure of ~1% across the structure of interest and are therefore not considered as significant for this study. Data from the Analog Fluxgate Magnetometer are used here [Russell et al., 2016].

2.1. Event Overview

Several small-scale magnetic holes are observed by the MMS constellation in the central plasma sheet near 0610 UT. Plasma data averaged to 0.3 s to improve counting statistics from MMS3 for this interval are shown in Figure 1 along with time-shifted (see section 2.2) 60 ms FGM data from all four observatories. Each small depression in magnetic field magnitude is observed by no more than two spacecraft at a time (Figure 1g). The largest of the depressions is observed around 06:10:50 by MMS3 and MMS4. The MMS3 ion moments are constant throughout this interval, and their overall flow speed is small (<30 km/s). The average density and temperature of ions are $\sim 3 \text{ cm}^{-3}$ and $\sim 1700 \text{ eV}$, respectively. Enhanced electron density and temperature inside the structure are due to an increased perpendicular electron pressure of $\sim 0.02 \text{ nPa}$ (Figure 1f). For this interval, the thermal gyroradii of electrons and ions are $\sim 2 \text{ km}$ and $\sim 300 \text{ km}$, respectively.

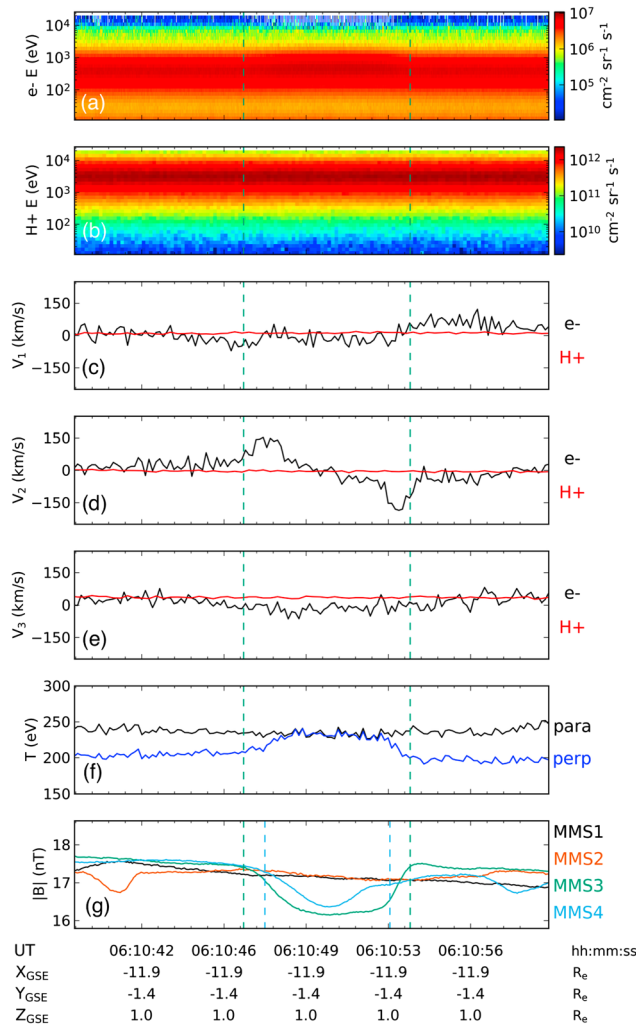


Figure 1. MMS plasma and magnetic field data of subproton-scale magnetic hole on 7 May 2015 at 06:10:50 UT near-local midnight. Burst plasma data are averaged to 0.3 s time resolution. (a) Electron energy-time spectrogram from MMS3/DES, (b) ion energy-time spectrogram from MMS3/DIS, (c–e) Bulk velocity from MMS3/FPI projected into (V_1, V_2, V_3) coordinates with $\mathbf{V}_1 = (0.60, 0.62, -0.51)$, $\mathbf{V}_2 = (-0.75, 0.20, -0.64)$, and $\mathbf{V}_3 = (-0.30, 0.76, 0.58)$. (f) Parallel and perpendicular electron temperature from MMS3/DES. (g) Magnetic field data from FGM for all four MMS spacecraft. Data are time shifted to line up with MMS3 by 9.9 s, 4.3 s, and 4.8 s, for MMS1, MMS2, and MMS4, respectively. Green and blue vertical dashed lines denote the boundaries of the primary magnetic hole as seen by MMS3 and MMS4, respectively. The structure is not observed in either MMS1 or MMS2. Other nearby magnetic depressions can be seen in adjacent spacecraft. The nominal interspacecraft spacing for the MMS constellation during this time period is 160 km.

$\mathbf{V}_i = (0, 33, 16)$ km/s to find \mathbf{V}_{MH} . For each candidate velocity vector, we transform the spacecraft positions into (X_1, X_2) coordinates and use a least-squares fit of the crossings of MMS3 and MMS4 to a circle. As shown in Figure 2, we find that $\mathbf{V}_{MH} = (-5.5, 35.5, 15.0)$ km/s provides a frame consistent with a ~70 km diameter cylindrical structure observed by the two spacecraft. The center location of the structure $(X_1, X_2) = (1.8, 8.8)$ km is also determined from this least-squares fit. The radial distance of each spacecraft from the center of the magnetic hole, R_{MH} , is calculated from this location. The time at which each spacecraft crosses the center line of the structure was used to time shift the data in Figure 1 to align their observations with MMS3. The structure is sufficiently small such that MMS1 and MMS2 do not observe corresponding magnetic depressions.

Bulk velocities from MMS3 are transformed (see section 2.2) from despun spacecraft coordinates (within a few degrees of true Geocentric Solar Ecliptic (GSE) coordinates) to (V_1, V_2, V_3) coordinates, where the \mathbf{V}_3 vector is parallel to the background magnetic field, $\mathbf{V}_1 = -\mathbf{V}_{MH} \times \mathbf{B}$ where \mathbf{V}_{MH} is the convection velocity of the magnetic hole (discussed in section 2.2), and \mathbf{V}_2 completes the right-handed system. A significant bipolar flow signature in the electrons appears perpendicular to the background field (Figure 1d). The statistical error in these averaged velocity peaks (see Gershman et al. [2015]) is less than 10%.

2.2. Mapping of Magnetic Structure

Mapping techniques using observations from four spacecraft have previously been used to calculate the propagation velocity and shape of subproton-scale magnetic holes (e.g., Sundberg et al. [2015]). Many magnetic holes were found to have cylinder-like structure and to propagate near the background ion flow speed. We build upon the results of these previous studies to enable the transformation of data from only two spacecraft (MMS3 and MMS4) into the reference frame of the magnetic hole, defined by coordinates (X', Y', Z') . Data from each spacecraft are transformed by $\mathbf{R}' = \mathbf{R} - (\mathbf{R}_o + \mathbf{V}_{MH}(t - t_o))$, where \mathbf{R}' and \mathbf{R} denote the vectors (X', Y', Z') and (X, Y, Z) in GSE, respectively, \mathbf{R}_o is a reference location of MMS3 at time $t_o = 06:50:50$ UT, and \mathbf{V}_{MH} is the velocity of the structure in GSE. We then project \mathbf{R}' into the plane perpendicular to the background magnetic field (defined by \mathbf{V}_1 , \mathbf{V}_2 , and \mathbf{V}_3 as described above) to obtain coordinates (X_1, X_2) .

We use a three-dimensional grid search around the average ion flow velocity

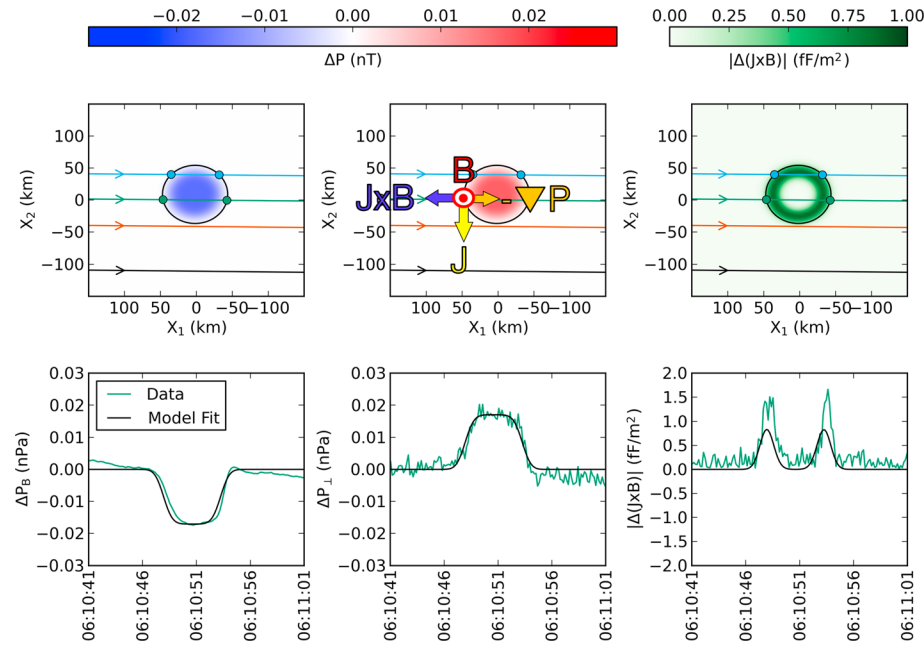


Figure 2. Structure of a subproton-scale magnetic hole as observed by MMS. (top row) Spacecraft position (MMS1 = black, MMS2 = red, MMS3 = green, and MMS4 = blue) in (X_1 , X_2) coordinates. The boundary of the magnetic hole is indicated with a black circle. Modeled fits of ΔP_B , ΔP_e , and $|\Delta(\mathbf{J} \times \mathbf{B})|$ are shown in Figures 2 (top left), 2 (top middle), and 2 (top right), respectively. For a structure in equilibrium, an electron pressure gradient is balanced by a $\mathbf{J} \times \mathbf{B}$ force generated by an azimuthally directed current. (bottom row) MMS3 observations and modeled fits that correspond to Figure 2 (top row). Good agreement between the MMS3 measurements and the model fit demonstrate that the observed structure is consistent with a quasi-cylindrical structure in equilibrium.

The magnetic and electron pressures as measured by MMS3 as a function of radial distance from the center of the hole are shown in Figure 2. Here the increase in perpendicular electron pressure balances the decrease in magnetic pressure. The parallel electron pressure remains unchanged throughout the structure (Figure 1f). A nonlinear least-squares fit of the form $\Delta P_e(R_{MH}) = a(1 - \text{erf}((R_{MH} - c)/b))$ to the perpendicular electron pressure data provides a direct estimate of the peak pressure change ($2a = 0.017$ nPa), current layer thickness ($b = 11$ km), structure radius ($c = 35$ km), and pressure gradient. Here the symbol Δ denotes a quantity taken relative to its average value at radial distances (R_{MH}) between 50 and 75 km. For a pressure-balanced magnetic hole (i.e., $\Delta P_B = -\Delta P_e$), we expect $\mathbf{J} \times \mathbf{B} = \nabla P$ such that an azimuthal current around the structure balances the pressure gradient. Comparisons of this model fit with MMS3-measured ΔP_B , ΔP_e , and $|\Delta(\mathbf{J} \times \mathbf{B})|$ quantities are shown in Figure 2. While not perfectly cylindrical as evidenced by some small distortions and asymmetries, the data show remarkable agreement with 2-D magnetohydrodynamic equilibrium at the electron level.

3. Current Layer Characterization

In addition to using plasma moments to investigate pressure balance, analysis of the distribution function of electrons can be used to characterize the properties of the current layer. Several angle-angle plots of MMS3-measured electrons around the magnetic hole are shown in Figure 3. Throughout the entire interval, the thermal plasma (below ~ 200 eV) shows enhanced flux parallel to the magnetic field, consistent with the $T_{||} > T_{\perp}$ measured outside of the magnetic hole and unchanged parallel pressure throughout the entire interval. Inside the structure, there is an enhancement of 90° pitch angle electrons limited to energies between ~ 200 eV and ~ 3000 eV (Figure 3c). This population is responsible for the increased perpendicular pressure shown in Figures 1 and 2. On the edges of the structure (Figures 3b and d), this 90° pitch angle distribution is agyrotropic in the spacecraft frame, i.e., the phase space density is not uniform along the dashed black line. On the leading and trailing edges, the location of the peak flux reverses direction. This agyrotropic population carries the current around the magnetic hole and is responsible for the bipolar peaks in the velocity shown in Figure 1d. The largest contributions to the electron velocity peaks are at ~ 1500 eV. Finally, Figure 4 shows a cut of the distribution function perpendicular to the magnetic field both inside ($R_{MH} < 25$ km) and outside

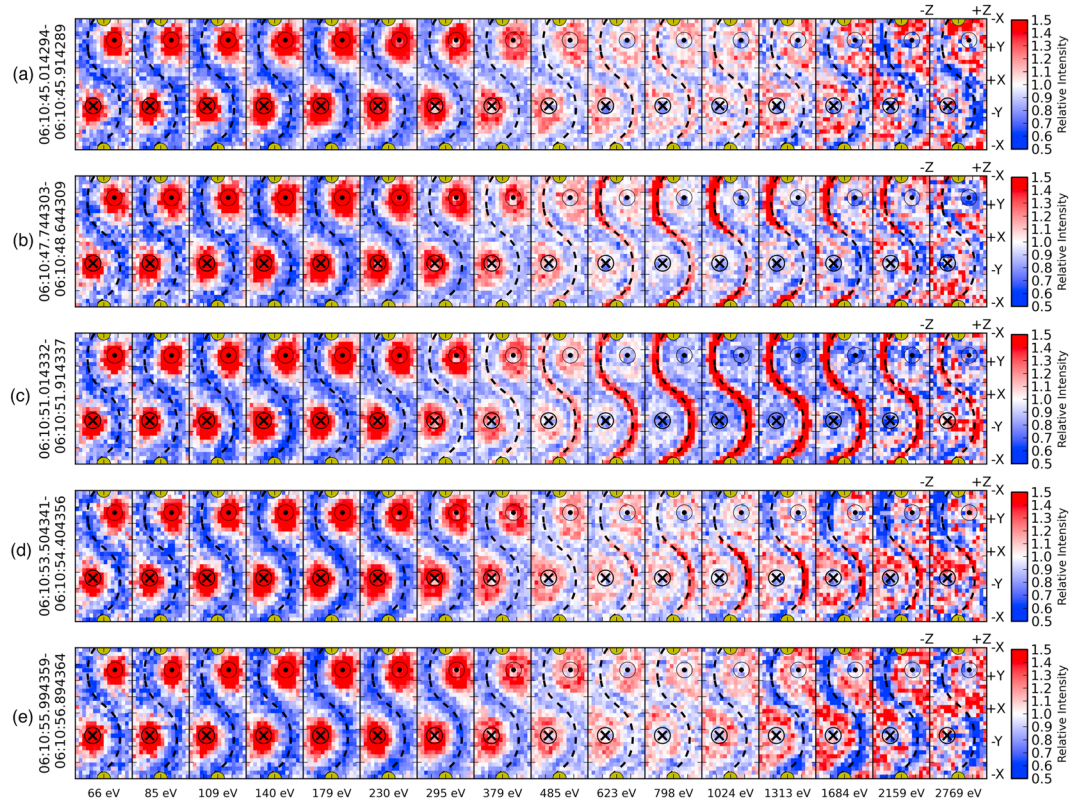


Figure 3. Angle-angle plots of MMS3/DES-measured phase space density from (a) before entering, (b) on the leading edge, (c) inside, (d) on the trailing edge, and (e) after exiting a subproton-scale magnetic hole. Circles with a “dot” and “crosses” denote particles flowing parallel to and antiparallel to the magnetic field, respectively. The black dashed line corresponds to particles with 90° pitch angles in the spacecraft frame. The yellow circle denotes particles flowing antisunward. Each energy bin is normalized by its average value to emphasize relative structure in each slice. Below the thermal energy (~200 eV), enhanced fluxes along the magnetic field are consistent with $T_{||} > T_{\perp}$. Inside the center of the structure, fluxes of electrons close to 90° pitch angles are substantially increased. At the leading and trailing edges of the magnetic hole, these 90° pitch angles are nongyrotropic. These agyrotropic electrons carry a current perpendicular to the magnetic field.

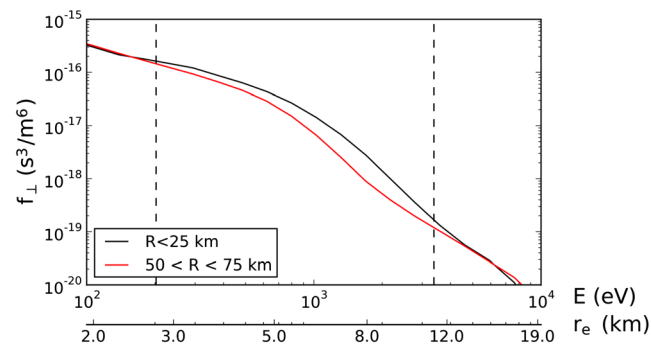


Figure 4. Phase space density perpendicular to the magnetic field as a function of energy and gyroradius for electrons inside the magnetic hole (black) and outside the magnetic hole (red). Perpendicular fluxes of electrons with energies between ~200 eV and ~3000 eV are enhanced inside ($R_{\text{MH}} < 25 \text{ km}$) the structure. These fluxes are well bracketed by the thermal gyroradius (leftmost vertical line) and the thickness of the current layer (rightmost vertical line) as determined from multispacecraft observations of the magnetic hole.

($50 \text{ km} < R_{\text{MH}} < 75 \text{ km}$) of the magnetic hole. The current carrying electrons have gyroradii between the thermal electron gyroradius ($\sim 2 \text{ km}$) and the current layer thickness ($\sim 11 \text{ km}$).

4. Discussion

Although $T_{||} \sim T_{\perp}$ inside this magnetic hole, the electrons are far from isotropic. This subtlety was also noted by analysis of similar structures with Cluster data [Sun et al., 2012; Sundberg et al., 2015]. The thermal plasma remains unchanged with significantly enhanced field-aligned fluxes and a constant $T_{||}$ throughout the structure. The trapped 90° pitch angle electrons provide a boost to the perpendicular

pressure, increasing T_{\perp} . The observed increase of temperature anisotropy is a kinetic-scale effect as opposed to that observed in analogous structures that are significantly larger than a proton gyroradius. In such fluid-scale structures, both the parallel and perpendicular fluxes of electrons are modified such that true isotropy is achieved [Balikhin et al., 2012].

Ambient plasma properties likely play an important role in the characteristic size of magnetic holes. A seed population of particles above the thermal speed is needed to form the current layer. The mass density of this population cannot grow too large relative to that of the thermal plasma, such that the net current that can be supported by a plasma is inherently limited. Cold or sparse plasmas may result in small-radius and weak-magnitude magnetic depressions. Such a scaling would further suggest that multiple holes in the same background plasma should have similar sizes. The other subproton-scale magnetic holes observed around this time interval are measured by only one or two spacecraft, consistent with this assertion.

Theoretical models of Bernstein-Green-Kusal (BGK) modes demonstrate that small-scale electron vortices are mathematically stable structures [Ng and Bhattacharjee, 2005; Eliasson and Shukla, 2007]. Such stability may explain why subproton-scale magnetic holes appear to naturally persist in both PIC simulations of turbulent relaxation and in the quiet plasma sheet. A reversed-polarity solution is also mathematically admissible and may correspond to electron phase space holes rather than magnetic holes [Ng and Bhattacharjee, 2005] but with equivalent geometry. Both types of BGK structures can generate an effective intermittency in the spatial structure of astrophysical plasmas [Haynes et al., 2015].

Finally, because ions are demagnetized throughout these structures, there is the potential for significant charge separation between electrons and ions. For the event showed here, there is only a small increase of the electron density inside the magnetic hole ($\sim 0.1 \text{ cm}^{-3}$) over the background density ($\sim 3 \text{ cm}^{-3}$). In deeper magnetic holes where the charge separation can be greater, large radial electric fields can be observed (K. A. Goodrich et al., MMS multi-point electric field observations of small-scale magnetic holes, submitted to *Geophysical Research Letters*, 2016). Large fields have also been reported in 2-D PIC models although they are not a necessary condition for the formation and sustaining of a subproton-scale magnetic hole [Haynes et al., 2015].

5. Concluding Remarks

FPI on MMS has sufficient resolution to characterize the current layers of small structures and truly study kinetic-scale plasma physics in a space environment. Detailed analysis of a subproton-scale magnetic hole at high resolution has revealed that agyrotropic electrons carry the current required to generate a $\sim 10\text{--}20\%$ diamagnetic depression in the background magnetic field. These electrons have gyroradii above the thermal gyroradius but below the current layer thickness. Consequently, the size and magnetic depth of kinetic-scale magnetic holes may be strongly dependent on the background plasma conditions. The electron-carried current observed for this event appears consistent with recent PIC simulations of turbulent relaxation, where small-scale magnetic holes naturally evolve out of $T_{\parallel} > T_{\perp}$ background plasma. The net motion of trapped electrons with $\sim 90^\circ$ pitch angles creates an azimuthal current that forms a self-consistent magnetic depression and can provide dissipation of injected magnetic energy at small scales.

Acknowledgments

The authors wish to thank the members of the FPI ground operations and science team for their feedback and support. This work was supported by the Magnetospheric Multiscale Mission under WBS 943396.05.03.02.10.01. IRAP contributions to MMS were funded by CNES and CNRS. Data used for this study are available from the MMS Science Data Center (<https://lasp.colorado.edu/mms/sdc/>).

References

- Amariutei, O. A., S. N. Walker, and T. L. Zhang (2011), Occurrence rate of magnetic holes between 0.72 and 1 AU: Comparative study of cluster and vex data, *Ann. Geophys.*, 29(5), 717–722, doi:10.5194/angeo-29-717-2011.
- Balikhin, M. A., D. G. Sibeck, A. Runov, and S. N. Walker (2012), Magnetic holes in the vicinity of dipolarization fronts: Mirror or tearing structures?, *J. Geophys. Res.*, 117, A08229, doi:10.1029/2012JA017552.
- Buti, B., B. T. Tsurutani, M. Neugebauer, and B. E. Goldstein (2001), Generation mechanism for magnetic holes in the solar wind, *Geophys. Res. Lett.*, 28, 1355–1358, doi:10.1029/2000GL012592.
- Cattaneo, M. B. B., C. Basile, G. Moreno, and J. D. Richardson (1998), Evolution of mirror structures in the magnetosheath of Saturn from the bow shock to the magnetopause, *J. Geophys. Res.*, 103, 11,961–11,972, doi:10.1029/97JA03683.
- Eliasson, B., and P. K. Shukla (2007), Theory for two-dimensional electron and ion Bernstein-Green-Kruskal modes in a magnetized plasma, *J. Plasma Phys.*, 73, 715–721, doi:10.1017/S0022377806006167.
- Fitzenreiter, R. J., and L. F. Burlaga (1978), Structure of current sheets in magnetic holes at 1 AU, *J. Geophys. Res.*, 83(A12), 5579–5585, doi:10.1029/JA083iA12p05579.
- Ge, Y. S., J. P. McFadden, J. Raeder, V. Angelopoulos, D. Larson, and O. D. Constantinescu (2011), Case studies of mirror-mode structures observed by THEMIS in the near-Earth tail during substorms, *J. Geophys. Res.*, 116, A01209, doi:10.1029/2010JA015546.
- Gershman, D. J., J. C. Dorelli, A. F. Viñas, and C. J. Pollock (2015), The calculation of moment uncertainties from velocity distribution functions with random errors, *J. Geophys. Res. Space Physics*, 120, 6633–6645, doi:10.1002/2014JA020775.
- Hasegawa, A. (1969), Drift mirror instability in the magnetosphere, *Phys. Fluids*, 12, 2642–2650.

- Haynes, C. T., D. Burgess, E. Camporeale, and T. Sundberg (2015), Electron vortex magnetic holes: A nonlinear coherent plasma structure, *Phys. Plasmas*, 22, 012309, doi:10.1063/1.4906356.
- Ng, C. S., and A. Bhattacharjee (2005), Bernstein-Green-Kruskal modes in a three-dimensional plasma, *Phys. Rev. Lett.*, 95, 245004.
- Pollock, C. J., et al. (2016), Fast plasma investigation for magnetospheric multiscale, *Space Sci. Rev.*, doi:10.1007/s11214-016-0245-4.
- Roytershteyn, V., H. Karimabadi, and A. Roberts (2015), Generation of magnetic holes in fully kinetic simulations of collisionless turbulence, *Phil. Trans. R. Soc., A*, 373, 20140151, doi:10.1098/rsta.2014.0151.
- Russell, C. T., W. Riedler, K. Schwingenschuh, and Y. Yeroshenko (1987), Mirror instability in the magnetosphere of comet Halley, *Geophys. Res. Lett.*, 14, 644–647, doi:10.1029/GL014i006p00644.
- Russell, C. T., L. K. Jian, J. G. Luhmann, T. L. Zhang, F. M. Neubauer, R. M. Skoug, X. Blanco-Canal, N. Omidi, and M. M. Cowee (2008), Mirror mode waves: Messengers from the coronal heating region, *Geophys. Res. Lett.*, 35, L15101, doi:10.1029/2008GL034096.
- Russell, C. T., et al. (2016), The Magnetospheric Multiscale magnetometers, *Space Sci. Rev.*, doi:10.1007/s11214-014-0057-3.
- Stevens, M. L., and J. C. Kasper (2007), A scale-free analysis of magnetic holes at 1 AU, *J. Geophys. Res.*, 112, A05109, doi:10.1029/2006JA012116.
- Sun, W. J., et al. (2012), Cluster and TC-1 observation of magnetic holes in the plasma sheet, *Ann. Geophys.*, 30, 583–595, doi:10.5194/angeo-30-583-2012.
- Sundberg, T., D. Burgess, and C. T. Haynes (2015), Properties and origin of subproton-scale magnetic holes in the terrestrial plasma sheet, *J. Geophys. Res. Space Physics*, 120, 2600–2615, doi:10.1002/2014JA020856.
- Tsurutani, B. T., D. J. Southwood, E. J. Smith, and A. Balogh (1992), Nonlinear magnetosonic waves and mirror mode structures in the March 1991 Ulysses interplanetary event, *Geophys. Res. Lett.*, 19(12), 1267–1270, doi:10.1029/92GL00782.
- Tsurutani, B. T., B. Buti, C. Galvan, J. K. Arballo, D. Winterhalter, R. Sakurai, G. S. Lakhina, E. J. Smith, and A. Balogh (2002), Relationship between discontinuities, magnetic holes, magnetic decreases, and nonlinear Alfvén waves: Ulysses observations over the solar poles, *Geophys. Res. Lett.*, 29(11), 1528, doi:10.1029/2001GL013623.
- Tsurutani, B. T., G. S. Lakhina, O. P. Verkhoglyadova, E. Echer, F. L. Guarnieri, Y. Narita, and D. O. Constantinescu (2011), Magnetosheath and heliosheath mirror mode structures, interplanetary magnetic decreases, and linear magnetic decreases: Differences and distinguishing features, *J. Geophys. Res.*, 116, A02103, doi:10.1029/2010JA015913.
- Turner, J. M., L. F. Burlaga, N. F. Ness, and J. F. Lemaire (1977), Magnetic holes in the solar wind, *J. Geophys. Res.*, 82(13), 1921–1924, doi:10.1029/JA082i013p01921.
- Winterhalter, D., M. Neugebauer, B. E. Goldstein, E. J. Smith, S. J. Bame, and A. Balogh (1994), Ulysses field and plasma observations of magnetic holes in the solar wind and their relation to mirror-mode structures, *J. Geophys. Res.*, 99(A12), 23,371–23,381, doi:10.1029/94JA01977.